PNAS RESEARCH ARTICLE | CELL BIOLOGY

RGMb drives macrophage infiltration to aggravate kidney disease

Yonglun Kong[a,b], Ming Yue[c], Chunhua Xu[d], Jing Zhang[e], Huiling Hong[a], Jiahuan Lu[a], Yang Wang[a], Xiaoyi Zhang[a], Qiuju Chen[a], Chen Yang[f], Hua-Feng Liu[f], Jinzhong Qin[g], Jingying Zhou[a], Nam Y. Lee[h], Bin Lin[e], Xiaoyu Tian[a], Gordon J. Freeman[i], and Yin Xia[a,b,j,1]

Affiliations are included on p. 11.

Edited by Martin Pollak, Beth Israel Deaconess Medical Center, Brookline, MA; received September 15, 2024; accepted February 3, 2025

The importance of macrophages in kidney diseases has been well established; however, the mechanisms underlying the infiltration of macrophages into injured kidneys are not well understood. RGMb is a member of the repulsive guidance molecule (RGM) family. RGMb can be expressed on the cell surface but a large portion of RGMb is localized intracellularly. Among various immune cell types, macrophages express the highest levels of RGMb, but the biological functions of RGMb in macrophages remain largely unknown. We find that RGMb promoted macrophage migration in vitro and that in vivo, RGMb enhanced infiltration of macrophages into injured kidneys and aggravated kidney inflammation and injury in mice. Mechanistically, RGMb bound to TAB1 inside the cell and facilitated the interaction between TRAF6 ubiquitin ligase and TAB1, thereby promoting TRAF6-mediated K63-linked polyubiquitination and phosphorylation of TAK1, followed by increased αTAT1 phosphorylation and α-tubulin acetylation. The resulting changes in the cytoskeleton promoted macrophage migration in vitro and in vivo. Deletion of Rgmb in macrophages markedly reduced TAK1 phosphorylation, αTAT1 phosphorylation, and α-tubulin acetylation and attenuated macrophage infiltration, renal inflammation, tubular injury, and interstitial fibrosis during kidney injury. Our results suggest that macrophage RGMb promotes kidney disease by increasing macrophage infiltration via the TRAF6-TAB1-TAK1/αTAT1/α-tubulin cascade.

kidney disease | RGMb | macrophage migration | kidney inflammation | TAB1

Significance

Macrophages are well known to be key players in kidney injury, inflammation, and fibrosis. However, the mechanisms underlying the infiltration of macrophages into injured kidneys are largely unknown. We now find that RGMb binds to TAB1 to enhance the interaction between TRAF6 and TAB1 and activate the TAK1/αTAT1/α-tubulin pathway, thereby promoting the infiltration of macrophages into the injured kidney and aggravating renal inflammation, injury, and fibrosis.

Acute kidney injury (AKI) affects up to 15% of all hospitalized patients and up to 50% of intensive care unit patients and is associated with a fourfold increase in mortality. Severe and persistent AKI leads to chronic kidney disease (CKD) that affects around 10% of the population worldwide. CKD can eventually progress to end-stage kidney disease and is also a strong risk factor for cardiovascular disease. CKD is estimated to become the fifth leading cause of death worldwide by 2040. Over the last 20 y, no new drug has been approved to specifically treat AKI and CKD due to a lack of understanding of the underlying mechanisms. Despite the differences between AKI and CKD regarding the causes and symptoms, AKI and CKD share common mechanisms including renal inflammation and tubular cell death (1–3).

Renal inflammation is the initial response to kidney injury, and it aims to resolve such an injury. However, overactive inflammatory responses destroy kidney structure and impair kidney function. Kidney injury induces accumulation and activation of inflammatory cells, and one of the major cell types is the macrophage. Macrophages and other cells produce proinflammatory cytokines, chemokines, and growth factors that induce tubular atrophy, glomerulosclerosis, microvascular rarefaction, and renal fibrosis (4, 5).

Repulsive guidance molecule b (RGMb) is a member of the RGM family, which consists of RGMa, RGMb (Dragon), and RGMc (hemojuvelin). The RGM proteins associate with cell membranes through a glycosylphosphatidylinositol (GPI) anchor and have been shown by us and others to be coreceptors for BMP signaling as well as ligands for the neogenin receptor (6). Interestingly, a substantial proportion of RGMb is localized inside the cell (7–9) due to high levels of clathrin-dependent endocytosis of cell surface RGMb (9) and alternative splicing (10, 11), but the role of intracellular RGMb has not been investigated.

The biological functions of RGMb are only beginning to emerge. Our previous study has revealed that homozygous Rgmb-deficient mice die at early postnatal ages (12). We also have demonstrated that RGMb is highly expressed in renal tubular cells and regulates tubular cell apoptosis and necroptosis during kidney injury (13, 14). In addition, RGMb binds to PD-L2 but not PD-L1 (7). Blockade of the PD-L2-RGMb interaction inhibited the development of respiratory tolerance by impairing the initial expansion of $CD4^+$ T cells (7). Blockade of the interactions between PD-L2 on dendritic cells and RGMb on

Author contributions: Y.K., H.-F.L., J.Q., B.L., X.T., G.J.F., and Y.X. designed research; Y.K., M.Y., C.X., J. Zhang, H.H., J.L., Y.W., X.Z., Q.C., C.Y., J. Zhou, and Y.X. performed research; J.Q., J. Zhou, N.Y.L., B.L., X.T., and G.J.F. contributed new reagents/analytic tools; Y.K., M.Y., C.X., J. Zhang, H.H., J.L., Y.W., X.Z., Q.C., H.-F.L., and Y.X. analyzed data; and Y.K., C.Y., H.-F.L., J.Q., J. Zhou, N.Y.L., B.L., X.T., G.J.F., and Y.X. wrote the paper.

Competing interest statement: Out potential conflicts of interest are US Provisional Patent Application No. 63/583,035 filed on 5 September 2023 (Applicants: Y.X., Y.K., and X.Z.) and patent applications for targeting RGMb for cancer immunotherapy and asthma (G.J.F.). The other authors have declared that no conflict of interest exists.

This article is a PNAS Direct Submission.

[1]To whom correspondence may be addressed. Email: xia.yin@cuhk.edu.hk.

This article contains supporting information online at https://www.pnas.org/lookup/suppl/doi:10.1073/pnas.2418739122/-/DCSupplemental.

Published March 13, 2025.

T cells overcame microbiome-dependent resistance to PD-1 pathway inhibitors (15).

In the immune system, RGMb is more highly expressed in macrophages than in other cell types (7, 8, 12). Interestingly, two studies suggested that RGMb may promote inflammation in certain diseases (8, 16). This appears to contradict our previous results showing that inhibition of RGMb promoted IL-6 expression in cultured macrophages (12), and global Rgmb knockout induced spontaneous lung inflammation in postnatal mice (12) and aggravated DSS-induced intestinal inflammation in adult mice (17). These discrepancies highlight the necessity of dissecting the specific functions of RGMb in different immune cells.

Macrophage accumulation and activation in tissues can result in exacerbated inflammation and tissue damage. The mechanisms underlying macrophage infiltration during kidney injury are not well understood (4, 5). It is well established that cytoskeletons, such as actin filaments and microtubules, play important roles in cell migration. Microtubules are hollow cylinders made up of polymerized α- and β-tubulin dimers and form the cytoskeleton together with microfilaments and intermediate filaments. Microtubules control cell migration by undergoing assembly and disassembly, which are regulated by posttranslational modifications. Stabilization of microtubules caused by their acetylation, which occurs at the K40 residue of α-tubulin, is critically involved in cell migration (18–21). α-tubulin N-acetyltransferase 1 (αTAT1) is the major, if not sole, enzyme that specifically acetylates K40 in α-tubulin (22). Increased αTAT1 expression and α-tubulin acetylation have been found to be key regulators of cell migration (20, 21, 23–25). Notably, recent studies have demonstrated that TAK1 phosphorylates αTAT1 at Ser237, which subsequently acetylates α-tubulin (26). In the present study, we demonstrated that LysM-Cre-mediated Rgmb ablation led to a decrease in the number of infiltrating macrophages (IMs) in the kidney. Both full-length (FL) and intracellular RGMb promoted macrophage migration and infiltration in vitro and in vivo. RGMb interacted with TAB1, thereby promoting TRAF6-mediated K63-linked polyubiquitination and phosphorylation of TAK1, followed by increased αTAT1 phosphorylation and α-tubulin acetylation which promoted macrophage migration in vitro and in vivo. Our results suggest that intracellular interactions of RGMb with TAB1 facilitated macrophage infiltration into injured kidneys, thereby promoting renal inflammation, tubular injury, and interstitial fibrosis.

Results

Expression of Rgmb in Macrophages in Mice and Human Patients. Our previous work revealed that among the immune cells isolated from the lung, Rgmb is most highly expressed in macrophages, and barely detectable in neutrophils (12). In agreement with the previous observations, Rgmb mRNA levels were much higher in macrophages than in neutrophils isolated from thioglycolate-treated peritoneum (*SI Appendix*, Fig. S1*A*). Importantly, single-cell RNA seq (27) analysis revealed that macrophages in inflamed human kidneys expressed more RGMb than circulating monocytes in the same patients (*SI Appendix*, Fig. S1*B*). As shown by single nucleus RNA-seq (28), Rgmb mRNA expression in macrophages already increased 4 h after ischemia/reperfusion injury (IRI) compared to control mouse kidneys and remained high even 6 wk after IRI (*SI Appendix*, Fig. S1*C*). These results support a role of RGMb in macrophages.

Loss of Rgmb in Macrophages Alleviated Kidney Inflammation, Injury, and Fibrosis. We generated *Rgmb$^{f/f}$;LysM-Cre/WT* mice as macrophage knockout (mKO) mice and *Rgmb$^{wt/wt}$;LysM-Cre/WT* as controls. Rgmb mKO mice were grossly normal at baseline. Both RGMb mRNA and proteins in bone marrow–derived macrophages (BMDMs) (*SI Appendix*, Fig. S1 *D* and *E*) and RGMb proteins in peritoneal macrophages (*SI Appendix*, Fig. S1*F*) were dramatically decreased in Rgmb mKO mice compared to control mice, confirming the effectiveness of Rgmb deletion in macrophages. Flow cytometry analysis of peripheral blood revealed no differences between control and Rgmb mKO mice in the ratios of myeloid cells, monocytes, Ly6C^{lo} monocytes, Ly6C^{hi} monocytes, eosinophils, neutrophils, basophils, and lymphoid cells to CD45$^+$ cells (*SI Appendix*, Fig. S2), suggesting that myeloid deletion of Rgmb did not alter the overall immune cell differentiation.

We induced AKI by injecting mice with Cisplatin (20 mg/kg bw). Serum, urine, and kidney samples were collected 72 h after Cisplatin injection. Cisplatin-induced renal functional impairment was mitigated in Rgmb mKO mice (*SI Appendix*, Fig. S3*A*). As indicated by urine and kidney Ngal and periodic acid–Schiff (PAS) stain (*SI Appendix*, Fig. S3 *B* and *C*), tubular injury induced by Cisplatin in control mice was much alleviated in Rgmb mKO mice. mRNA levels of the inflammatory factors Il-6, Il-1β and Cxcl2 in the kidney were elevated by Cisplatin in control mice but were lower in Rgmb mKO mice (*SI Appendix*, Fig. S3*D*). Immunofluorescence showed that there was a decrease in the number of F4/80 positive macrophages in Rgmb mKO kidneys compared to control kidneys after Cisplatin treatment (*SI Appendix*, Fig. S3*E*). The number of S100a4 positive IMs (29) was also decreased in Rgmb mKO kidneys compared to control kidneys (*SI Appendix*, Fig. S3*F*).

In response to a higher dose of Cisplatin at 25 mg/kg, 76.9% of Rgmb mKO mice died within 5 d, which was lower than the death rate of 92.3% of control mice (*SI Appendix*, Fig. S4*A*). The 5-d death rates were much reduced at a lower dose of 15 mg/kg of Cisplatin compared to the dose of 25 mg/kg, and there were still fewer deaths in Rgmb mKO mice than in control mice (*SI Appendix*, Fig. S4*B*). In the mice that survived 5 d after injection of Cisplatin at 15 mg/kg, the elevated levels of creatinine and blood urea nitrogen (BUN) in control mice were much reduced in Rgmb mKO mice (*SI Appendix*, Fig. S4*C*). Tubular injury was much alleviated in Rgmb mKO mice (*SI Appendix*, Fig. S4 *D* and *E*). The elevated mRNA levels of Adgre1 (F4/80), Tnfα, Il6, and Cxcl2 in control mice were also attenuated in Rgmb mKO mice 5 d after Cisplatin administration (*SI Appendix*, Fig. S4*F*). Importantly, flow cytometry showed that the percentages of CD11b$^+$F4/80$^+$ macrophages in CD45$^+$ cells were much lower in Rgmb mKO than in control kidneys 5 d after Cisplatin treatment (*SI Appendix*, Fig. S5).

We then induced CKD by injecting mice with a low dose of Cisplatin (7.5 mg/kg) once a week for 4 wk. Renal function was less impaired in Rgmb mKO mice (Fig. 1*A*). Tubular injury was also much mitigated in Rgmb mKO mice (Fig. 1 *B* and *C*). The elevated mRNA levels of both proinflammatory (Tnf-α and Cxcl2) and anti-inflammatory factors (Arg1 and Tgfβ1) in control mice were diminished in Rgmb mKO mice (*SI Appendix*, Fig. S6 *A* and *B*). mRNA levels of Adgre1 (F4/80) in the kidney (*SI Appendix*, Fig. S6*C*) and F4/80 positive macrophage numbers (Fig. 1*D*) were increased by Cisplatin treatments in control mice, which were much decreased in Rgmb mKO mice. mRNA levels of the fibrosis markers Acta2, Col1, Col3, Col4, and Fn-1 and protein levels of α-SMA and Col1 (*SI Appendix*, Fig. S6 *D* and *E*) were all increased in Cisplatin-treated control kidneys, and they were reduced in Rgmb mKO kidneys. Consistently, Masson's trichrome staining (MTS) showed much decreased interstitial fibrosis in Rgmb mKO compared to control kidneys (Fig. 1*E*).

We also performed unilateral ischemia–reperfusion injury followed by contralateral nephrectomy (uIRx). The impaired renal function and increased inflammation, macrophage infiltration, and fibrosis induced by uIRx in control mice were all mitigated in Rgmb mKO mice (*SI Appendix*, Fig. S7).

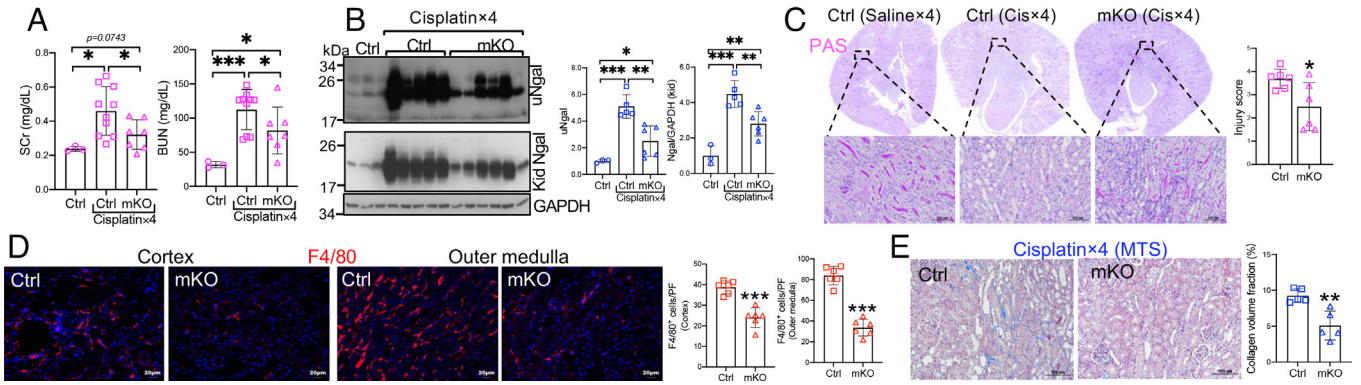

Fig. 1. Myeloid Rgmb deletion alleviated CKD induced by multiple low doses of Cisplatin. Male Rgmb mKO (*Rgmb*$^{flox/flox}$*;LysM-Cre/WT*) and control (*LysM-Cre/WT*) mice at 2 mo of age were used. Mice were injected with saline or Cisplatin at 7.5 mg/kg bw once a week for 4 wk (Cisplatin×4). Serum creatinine and BUN levels (*A*), Ngal levels in the urine and kidney (*B*), PAS staining and tubular injury scores (n = 6 mice, *C*), immunofluorescence for F4/80$^+$ cells (n = 6 mice, *D*), and Masson's trichrome staining (MTS) (n = 5 mice, *E*) are presented. GAPDH was used as the loading control for western blotting. Rpl19 was used as the internal control for real-time PCR. *$P < 0.05; **$P < 0.01; ***$P < 0.001.

In response to unilateral ureteral obstruction for 7 d (UUO 7d), mRNA levels of both proinflammatory factors and the anti-inflammatory factors were elevated in control mice, which were lowered in Rgmb mKO mice. The increased expression of fibrosis markers in control mice was also attenuated in Rgmb mKO mice at both 7 and 10 d of UUO (*SI Appendix*, Fig. S8). These results collectively suggest that deletion of Rgmb in the myeloid lineage leads to decreases in macrophage infiltration, kidney inflammation, tubular injury, and interstitial fibrosis during AKI, AKI-to-CKD transition, and CKD.

Loss of Rgmb in Macrophages Protected Against Sepsis. The kidney is one of the most commonly affected organs in sepsis. We induced sepsis by lipopolysaccharide (LPS) injection in control and Rgmb mKO mice, followed by monitoring for 7 d. All 10 Rgmb mKO mice survived, whereas 4 out of the 8 control mice died after LPS treatment (*SI Appendix*, Fig. S9*A*). Notably, F4/80 positive macrophage numbers were decreased not only in the kidneys and but also in the livers of Rgmb mKO mice compared to those of control mice after LPS treatment (*SI Appendix*, Fig. S9 *B* and *C*). Rgmb mKO mice were also highly protected against sepsis induced by cecal ligation and puncture (CLP) (*SI Appendix*, Fig. S9*D*).

IM Numbers Were Decreased in the Kidneys of Rgmb mKO Mice. Two major populations of macrophages, i.e., kidney resident macrophages (KRMs) and IMs, are present in the kidney and can be classified on the basis of the cell surface markers F4/80 and CD11b in mice (30). To examine the effects of LysM-Cre mediated Rgmb deletion on IMs and KRMs, we first performed flow cytometry to determine the numbers of IMs and KRMs in Rgmb mKO and control mice under basal conditions. RGMb expression in IMs (CD45$^+$GR-1$^-$ CD11b^{hi}F4/80^{low}) was lower in Rgmb mKO mice than in control mice (*SI Appendix*, Fig. S10 *A*, *Left*, and *B*). IM numbers in the kidney were also decreased in Rgmb mKO mice when compared to control mice (*SI Appendix*, Fig. S10 *A*, *Right*). In contrast, RGMb expression in KRMs (CD45$^+$GR-1$^-$ CD11b^{mid}F4/80^{hi}) did not differ between the two genotypes (*SI Appendix*, Fig. S10 *B* and *C*, *Left*). The KRM numbers tended to be lower in Rgmb mKO mice than in control mice (*SI Appendix*, Fig. S10 *C*, *Right*). These results suggest that LysM-Cre-mediated Rgmb ablation reduced the number of IMs and their expression of RGMb.

To further characterize macrophage infiltration, we performed scRNA-seq on the kidneys of WT and Rgmb mKO mice at baseline and 72 h after Cisplatin injection. Unsupervised clustering of the aggregated data from 13,200 cells identified 11 discrete clusters based on the representative marker genes in murine kidneys (*SI Appendix*, Fig. S10 *D* and *E*) (31–33). Differential proportional analysis showed that the proportions of Cx3cr1$^+$ and Ccr2$^+$ IMs in the kidney were lower in Rgmb mKO mice than in WT mice (1.85 vs. 3.54%) at baseline (*SI Appendix*, Fig. S10 *F* and *H*). The proportions of IMs increased after Cisplatin treatment, but they were still much lower in Rgmb mKO mice than in WT mice (2.35% vs. 10.1%) (*SI Appendix*, Fig. S10*F*). Notably, the proportions of the resident macrophages, identified by the typical markers such as C1qa, C1qc, and Cd74, were similar between Rgmb mKO and WT mice both at baseline (1.83% vs. 1.75%) and after Cisplatin treatment (5.94% vs. 5.63%) (*SI Appendix*, Fig. S10 *F* and *H*). The proportions of proximal tubular (PT) cells were decreased by Cisplatin, but they were higher in Rgmb mKO mice than in WT mice (*SI Appendix*, Fig. S10*F*), which aligned with the alleviated tubular injury in Rgmb mKO mice (*SI Appendix*, Fig. S3 *B* and *C*). These results indicate that LysM-Cre-mediated Rgmb ablation decreased the amount of macrophage infiltration but had no major effects on resident macrophages.

Maf, Mafb, Rbpj, Mif, Egr-1, and Gbx2 have been reported to promote monocyte-to-macrophage differentiation (33–36). We found no significant changes in the expression of those genes in IMs between WT and Rgmb mKO mice after Cisplatin treatment (*SI Appendix*, Fig. S10*G*). Therefore, RGMb may not regulate the differentiation of IMs during kidney injury.

RGMb Promoted Macrophage Migration and Invasion In Vitro and In Vivo. Because of the decreased amount of macrophage infiltration in the injured kidneys of Rgmb mKO mice, we investigated effects of RGMb on macrophage migration in vitro. We isolated BMDMs from control and Rgmb mKO mice. 90% of the cells were found to be F4/80 and CD45 double positive, with minimal apoptosis (*SI Appendix*, Fig. S11). As shown by Transwell migration assay, the chemotactic responses to 10% FBS, CX3CL1, CCL19, or fMLP were drastically decreased in Rgmb mKO BMDMs compared with control BMDMs (Fig. 2*A*). Inhibition of RGMb expression by siRNA markedly reduced the migration of RAW264.7 macrophages toward 10% FBS (Fig. 2*B* and *SI Appendix*, Fig. S12*A*) while overexpression of RGMb time-dependently promoted the migration of RAW264.7 cells (Fig. 2*C* and *SI Appendix*, Fig. S12*B*). Deletion of Rgmb also significantly decreased the ability of BMDMs to migrate in the wound healing assay (*SI Appendix*, Fig. S13*A*), and overexpression of RGMb promoted the wound healing of RAW264.7 cells (*SI Appendix*, Fig. S13*B*). In addition, deletion of

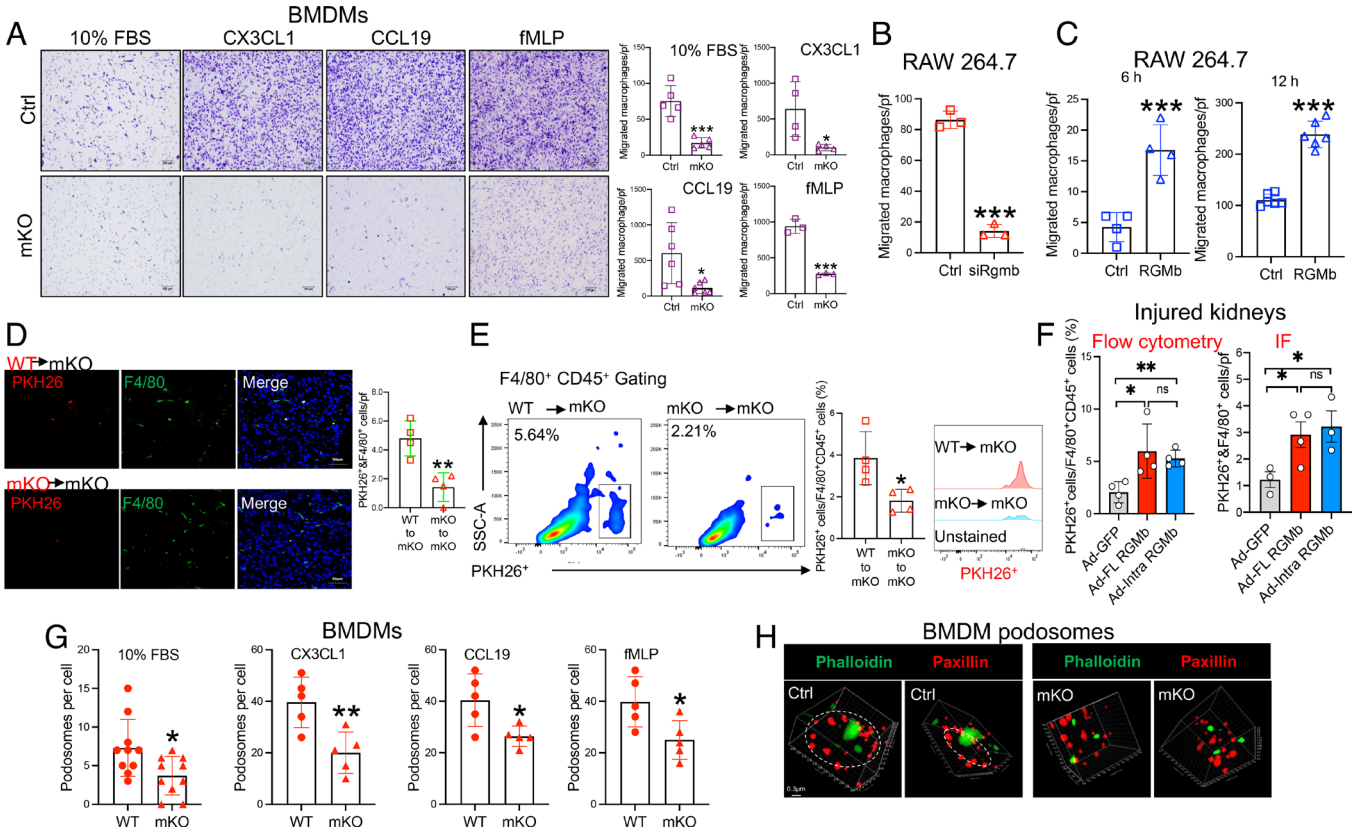

Fig. 2. Rgmb promoted macrophage migration and invasion in vitro and in vivo and facilitated podosome formation in vitro. (*A*) 3 × 10^5 BMDMs from control and Rgmb mKO mice were seeded on Transwell insert in the upper chamber. 10% FBS, CX3CL1 (100 ng/mL), CCL9 (100 ng/mL), or fMLP (250 μM) were added into the lower chamber. 6 h later, migrated cells were counted. One well represents one animal. (*B*) RAW264.7 macrophages were transfected with control siRNA or Rgmb siRNA. 3 × 10^5 cells were seeded on Transwell insert. 10% FBS was added into the lower chamber. 12 h later, migrated cells were counted. n = 3 wells. (*C*) RAW264.7 macrophages were transfected with control plasmids or Rgmb plasmids. Migration assays for 6 or 12 h were performed. (*D* and *E*) In vivo migration assay: PKH26 labeled control or Rgmb mKO BMDMs were injected through the tail vein into Rgmb mKO mice. Two days later, the mice were injected with Cisplatin. Labeled macrophages in the kidney were evaluated 3 d after Cisplatin by immunofluorescence for F4/80 (*D*) or flow cytometric analysis for F4/80 and PKH26 double-positive cell numbers (*E*). Only one of the three flow cytometry repeats is presented. Refer to *SI Appendix*, Fig. S16*B* for the three repeats. n = 4 mice. (*F*) Rgmb mKO BMDMs were infected with Ad-GFP, Ad-FL RGMb, or Ad-Intra RGMb before they were labeled with PKH26 and injected through the tail vein into Rgmb mKO mice. Two days later, the mice were injected with Cisplatin. Labeled macrophages in the injured kidney were evaluated 3 d after Cisplatin injection by flow cytometry (*Left* panel) or immunofluorescence (*Right* panel). n = 4 mice. (*G*) Deletion of Rgmb reduced podosome numbers in BMDMs. BMDMs from control and Rgmb mKO mice were seeded on fibronectin-coated coverslips and exposed to 10% FBS, CX3CL1, CCL19, or fMLP for 1 h. Podosomes were counted in individual cells. n = 5 or 10 cells. (*H*) 3D reconstruction of podosomes by STED microscopy in control and Rgmb mKO BMDMs exposed to CX3CL1 for 1 h. **P* < 0.05; ***P* < 0.01; ****P* < 0.001.

Rgmb decreased the invasion of BMDMs into Matrigel in response to CX3CL1 or CCL19 (*SI Appendix*, Fig. S14).

The effects of Rgmb deletion on the migration of M1 and M2 macrophages were also studied. The migration was much decreased in Rgmb mKO BMDMs compared to control BMDMs after they had been induced into M1 macrophages by LPS or into M2 macrophages by IL-4 (*SI Appendix*, Fig. S15).

To investigate the role of RGMb in macrophage infiltration into injured kidneys in vivo, BMDMs from control or Rgmb mKO mice were labeled with the tracking dye PKH26. 2 × 10^6 PKH26-labeled cells were injected through the tail vein into Rgmb mKO mice 48 h before Cisplatin injection. Three days after Cisplatin injection, the numbers of PKH26 and F4/80 double-positive cells in the injured kidneys were evaluated (*SI Appendix*, Fig. S16*A*). As shown by immunofluorescence (Fig. 2*D*), there were significantly decreased numbers of PKH26 and F4/80 double-labeled Rgmb mKO macrophages compared to those of double-labeled WT macrophages in the injured kidneys. Flow cytometry also demonstrated that mice that had received PKH26-labeled Rgmb mKO BMDMs showed marked decreases in the injured kidney in the percentage of $PKH26^+$ macrophages in $F4/80^+CD45^+$ cells compared to control BMDMs (Fig. 2*E* and *SI Appendix*, Fig. S16*B*). Notably, adenovirus-mediated reconstitution of RGMb in Rgmb mKO BMDMs restored the migration of PKH26-labeled Rgmb mKO BMDMs into injured kidneys as indicated by flow cytometry (Fig. 2 *F*, *Left* panel, compare bars 2 and 1; *SI Appendix*, S17 *A and B*) and immunofluorescence (Fig. 2 *F*, *Right* panel, compare bars 2 and 1; *SI Appendix*, Fig. S18). Therefore, our results indicate that RGMb promotes macrophage migration and invasion both in vitro and in vivo.

RGMb Promoted Macrophage Migration Speed and Podosome Formation. We tracked the two-dimensional migration of macrophages seeded in 12-well plates. Deletion of Rgmb reduced the migration speed but had no effects on the directionality (displacement length ratio) in BMDMs (*SI Appendix*, Fig. S19 *A* and *B*). Conversely, RGMb overexpression increased the migration speed and again had no effects on the directionality in RAW264.7 cells (*SI Appendix*, Fig. S19 *C* and *D*).

Adhesion and migration of monocyte-derived cells are regulated by podosomes (37). Each podosome is about 0.5 to 2 μm in diameter and exhibits a distinct core (consisting of dot-like F-actin assemblies) and a ring (containing integrin receptors and adhesion adaptor proteins including paxillin, talin, and cortactin) (38). We performed costaining of F-actin (Phaloidin) and paxillin to visualize the podosomes of BMDMs cultured on fibronectin-coated coverslips and exposed to 10% FBS, CX3CL1, CCL19, or fMLP.

As revealed by confocal microscopy, podosome numbers were much reduced in Rgmb mKO BMDMs compared to control BMDMs (Fig. 2*G* and *SI Appendix*, Fig. S20*A*). At a higher magnification, a distinct F-actin core was surrounded by a paxillin ring in each of the podosomes in control BMDMs, whereas the rings of the podosomes in Rgmb mKO BMDMs showed discontinuity (*SI Appendix*, Fig. S20*B*). Fluorescence intensity analysis of paxillin and F-actin revealed each peak of F-actin is enclosed by two peaks of paxillin in control BMDMs. Such a pattern was barely observed in Rgmb mKO BMDMs (*SI Appendix*, Fig. S20*C*). Strikingly, under a stimulated emission depletion (STED) super-resolution microscope, the paxillin ring in control BMDMs was composed of evenly spaced paxillin punctuates that enclosed a protruded F-actin core. The paxillin punctuates were disorganized and no distinct F-actin core was observed in the podosomes of Rgmb mKO BMDMs (Fig. 2*H*).

Intracellular RGMb Drove Macrophage Migration Both In Vitro and In Vivo. The effects of RGMb on migration might be mediated by soluble, cell-surface, or intracellular RGMB. To test these possibilities, we collected conditioned medium (CM) from WT and Rgmb mKO BMDMs and added the CM into the lower chambers of Transwells to examine the migration ability of WT and Rgmb mKO BMDMs (*SI Appendix*, Fig. S21*A*). The migrated Rgmb mKO cell numbers were similar no matter whether they were exposed to fresh medium, WT CM, or mKO CM, and they were much lower than the numbers of migrated WT BMDMs exposed to either fresh medium or mKO CM (*SI Appendix*, Fig. S21*B*). Furthermore, BMDM migration toward 10% FBS was not altered by RGMb antibody treatment (*SI Appendix*, Fig. S21*C*). These results indicate that neither the soluble nor the cell surface RGMb regulated macrophage migration in our settings. We therefore hypothesized that intracellular RGMb drives macrophage migration. In this connection, we observed high levels of endogenous RGMb inside migrating RAW264.7 macrophages (*SI Appendix*, Fig. S21*D*).

We then generated an intracellular RGMb construct (Intra RGMb) by deleting the signal peptide. We confirmed that Intra RGMb is localized to the cytosol but not on the plasma membrane while FL RGMb was present on both (*SI Appendix*, Fig. S22). Strikingly, expression of Intra RGMb promoted RAW264.7 migration in vitro (Fig. 3*A* and *SI Appendix*, Fig. S23*B*). We reintroduced Intra RGMb or FL RGMb into Rgmb mKO BMDMs through adenovirus infection. Like FL RGMb, Intra RGMb restored Rgmb mKO BMDM migration in vitro (Fig. 3*B* and *SI Appendix*, Fig. S23*A*). We also used PKH26 to label Rgmb mKO BMDMs infected with Ad-GFP, Ad-FL RGMb, or Ad-Intra RGMb before the cells were injected into mice. We found that reconstitution of either Intra RGMb or FL RGMb promoted Rgmb mKO BMDM infiltration into the injured kidneys as shown by flow cytometry and immunofluorescence (Fig. 2*F* and *SI Appendix*, Figs. S17 and S18).

RGMb contains a proteolytic cleavage site between Asp171 and Pro172. After cleavage, the N-terminus and the C-terminus of RGMb remain connected by disulfide bonds. Interestingly, cotransfection of the C-terminus and the N-terminus of RGMb (C+N) into RAW264.7 macrophages also promoted migration although the N-terminus alone or the C-terminus alone did not (Fig. 3 *C* and *D* and *SI Appendix*, Fig. S23 *C* and *D*). Mutation of the cleavage site DP to AA (RGMb-DP/AA) did not alter the promigratory activity of RGMb (Fig. 3*D* and *SI Appendix*, Fig. S23*D*).

Both FL and Intracellular RGMb in Macrophages Promoted Kidney Injury. We used liposomal clodronate (CLD) to deplete macrophages in mice. Two doses of CLD reduced monocytes/

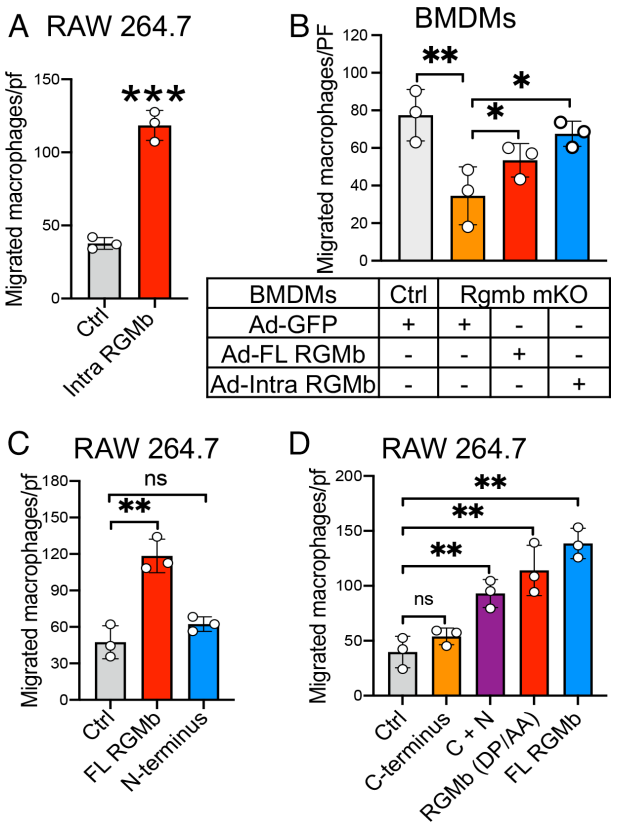

Fig. 3. Intracellular RGMb promoted macrophage migration. (*A*) Effects of intracellular RGMb (Intra RGMb) on the migration of RAW264.7 macrophages. Cells were transfected with pcDNA3.1 (Ctrl) or Intra RGMb plasmids. Twenty-four hours after transfection, 3×10^5 cells were seeded in a Transwell insert and were allowed for migration for 16 h. (*B*) Effects of reintroduction of FL RGMb or Intra RGMb on the migration of Rgmb mKO BMDMs. Rgmb mKO BMDMs were infected with Ad-FL RGMb or Ad-Intra RGMb before the cells were subjected to Transwell migration assay. (*C* and *D*) Effects of various RGMb mutations on the migration of RAW264.7 macrophages. n = 3 wells. $^*P < 0.05$; $^{**}P < 0.01$; $^{***}P < 0.001$.

macrophages in blood and spleen by 68.7% and 69.7%, respectively (*SI Appendix*, Fig. S24). As expected, renal dysfunction (Fig. 4*C*), inflammation (Fig. 4*D*), and tubular injury (Fig. 4 *E* and *F*) were induced by Cisplatin in mice injected with liposomal vehicle without CLD (group #1) (compare group #1 with group S), and they were all much attenuated when macrophages were depleted (compare group #2 with group #1). Transfer of macrophage-depleted mice with WT BMDMs (group #3) but not Rgmb mKO BMDMs (group 4) (Fig. 4 *A* and *B*) restored renal dysfunction (Fig. 4*C*), inflammation (Fig. 4*D*), and tubular injury (Fig. 4 *E* and *F*) (compare group #3 or #4 with group #1). Strikingly, reconstitution of Rgmb mKO BMDMs with either Intra RGMb (group #6) or FL RGMb (group #5) brought the renal functional impairment, renal inflammation, and tubular injury to the levels seen in macrophage-depleted mice transferred with WT BMDMs (Fig. 4 *C–F*, compare group #5 or #6 with group #3). These results indicate a critical role for RGMb in mediating macrophage migration and kidney injury and that intracellular localization of RGMb is sufficient for this function.

RGMb Interacted with TAB1 and Promoted the TRAF6-Mediated K63-Linked Polyubiquitination and Phosphorylation of TAK1. To understand the mechanisms used by RGMb to promote macrophage migration. We performed RGMb binding protein prediction by STRING database and found that TAB1 is one of the potential RGMb binding proteins (*SI Appendix*, Fig. S25*A*).

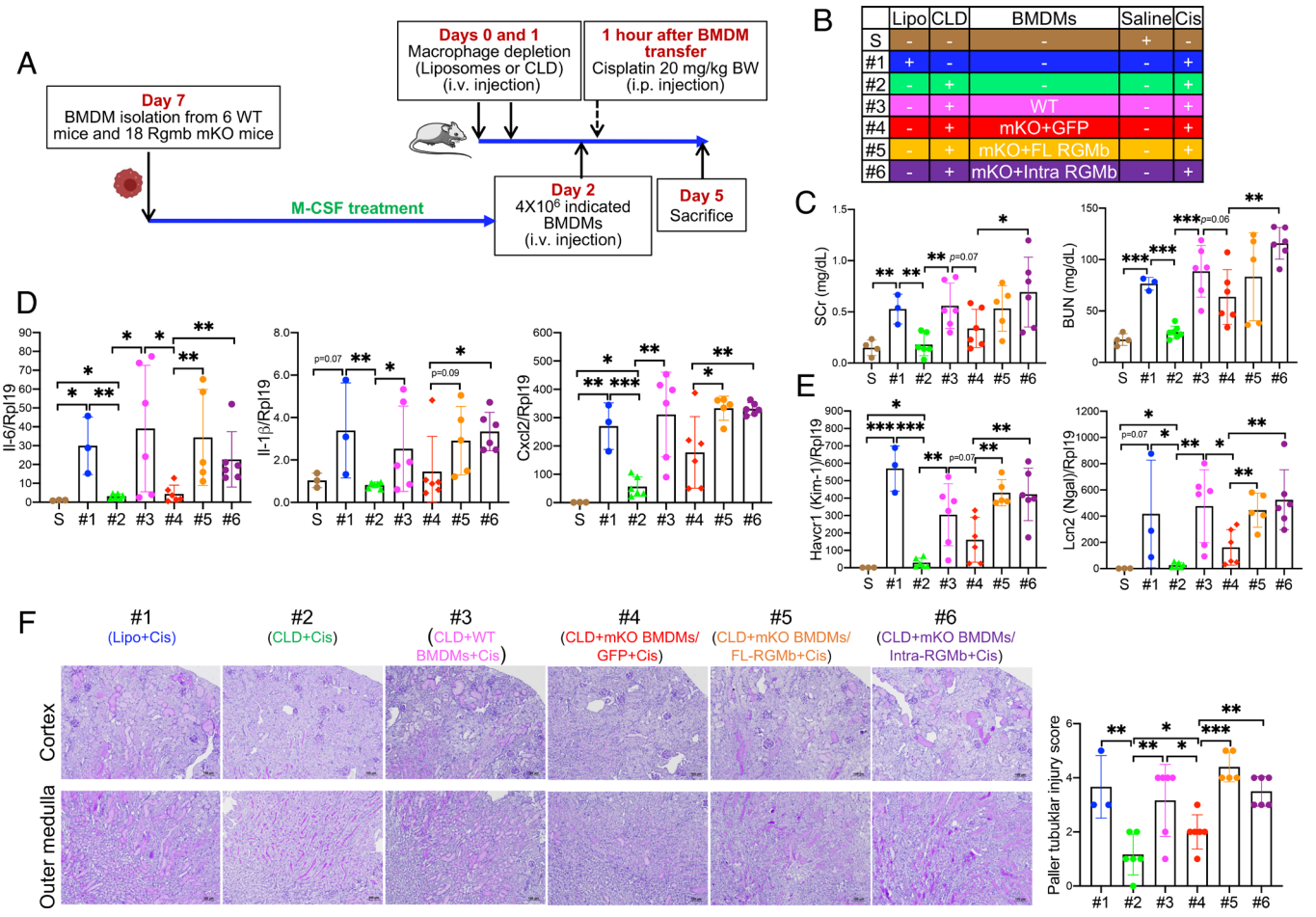

Fig. 4. RGMb in macrophages mediated kidney injury and intracellular expression of RGMb was sufficient for this function. (*A*) Schematic diagram of the experiment. BMDMs were obtained from WT and Rgmb mKO mice and were infected with Ad-GFP, Ad-Intra Rgmb, or Ad-FL Rgmb. Mice were injected via tail vein with liposomes or liposomal clodronate (CLD) (5 mg/mL) on day 0 and day 1, and then were injected via tail vein with or without BMDMs (4×10^6) as indicated on day 2, followed by saline or Cisplatin (i.p.) injection. Serum and kidney samples were collected on day 5. (*B*) Mouse grouping. The mouse groups used for the measurements in panels *C*–*F*. (*C*) Serum creatinine and BUN levels. (*D*) mRNA levels of Il-6, Il-1β and Cxcl2 in the kidney. (*E*) mRNA levels of Havcr1 (Kim1) and Lcn2 (Ngal) in the kidney. (*F*) PAS staining (*Left*) and tubular injury scores (*Right*). n = 3 to 6 mice. **P* < 0.05; ***P* < 0.01; ****P* < 0.001.

Immunoprecipitation-Mass Spectrometry (IP-MS) assay on lysates from control and stable 3×Flag-RGMb (Flag after signal and before RGMb) overexpressing RAW264.7 cells (*SI Appendix*, Fig. S25*B*) showed that TAB1 is one of the top 30 hits (Fig. 5*A*). Furthermore, 14 and 2 unique peptides were identified for TAB1 and RGMb respectively in the 3×Flag-RGMb eluate, while no TAB1 and RGMb peptide was found in the control eluate (*SI Appendix*, Fig. S25*C* and Dataset S1). RGMb binding proteins were highly enriched for posttranslational modification, cytoskeleton, and cell motility (*SI Appendix*, Fig. S25*D*).

We performed IP and reciprocal IP experiments and found that RGMb and TAB1 indeed were coprecipitated with each other when the two proteins were overexpressed in HEK293T cells (Fig. 5*B*). This interaction was confirmed by the PLA when 3×Flag-RGMb and TAB1-HA were overexpressed in RAW264.7 cells (Fig. 5*C*). Overexpressed RGMb coprecipitated endogenous TAB1 in stable 3×Flag-RGMb-overexpressing RAW264.7 cells (*SI Appendix*, Fig. S26*A*). Endogenous RGMb pulled down endogenous TAB1 in WT but not in Rgmb mKO BMDMs (*SI Appendix*, Fig. S26*B*). Of note, purified TAB1 (26) was coimmunoprecipitated with recombinant RGMb (*SI Appendix*, Fig. S26 *C* and *D*). These results suggest that RGMb directly interacted with TAB1. Interestingly, RGMb did not interact with TAB2 and TAB3 (*SI Appendix*, Fig. S26*E*), which are structurally and functionally related to TAB1 (39). Intracellular RGMb and the C-terminus of RGMb also interacted with TAB1 whereas the N terminus of RGMb did not (*SI Appendix*, Fig. S26*F*). Within the C-terminus, the fragment aa 172-336 containing partial vWF-D-like domain but not the fragment aa 337-436 interacted with TAB1 (*SI Appendix*, Fig. S26 *G*–*I*).

TAB1 constitutively interacts with TAK1 and participates in the regulation of K63-linked polyubiquitination of TAK1 (40, 41). Therefore, we examined the effects of RGMb on TAK1 polyubiquitination. We cotransfected Flag-TAK1 and RGMb into RAW264.7 cells along with HA-tagged wild-type ubiquitin. As shown by western blotting using anti-HA and anti-K63-Ub antibodies, TAK1 polyubiquitination, and K63-linked polyubiquitination both were dramatically enhanced by RGMb (Fig. 5*D*). We also used ubiquitin mutants containing one lysine only at position 63 (K63-only) or 48 (K48-only). RGMb increased the TAK1 polyubiquitination in the presence of wild-type Ub or the K63-only mutant but not the K48-only mutant (Fig. 5*E*). Therefore, RGMb promotes K63-linked polyubiquitination of TAK1. Note that K63 polyubiquitination serves as a scaffold for protein–protein interactions and regulates immune functions but does not promote degradation.

Both TNF receptor–associated factor 2 (TRAF2) and TRAF6 are RING-domain ubiquitin ligases that catalyze K63-linked polyubiquitination of TAK1 at the Lys158 residue, which then leads to TAK1 autophosphorylation and activation (41–43). X-linked

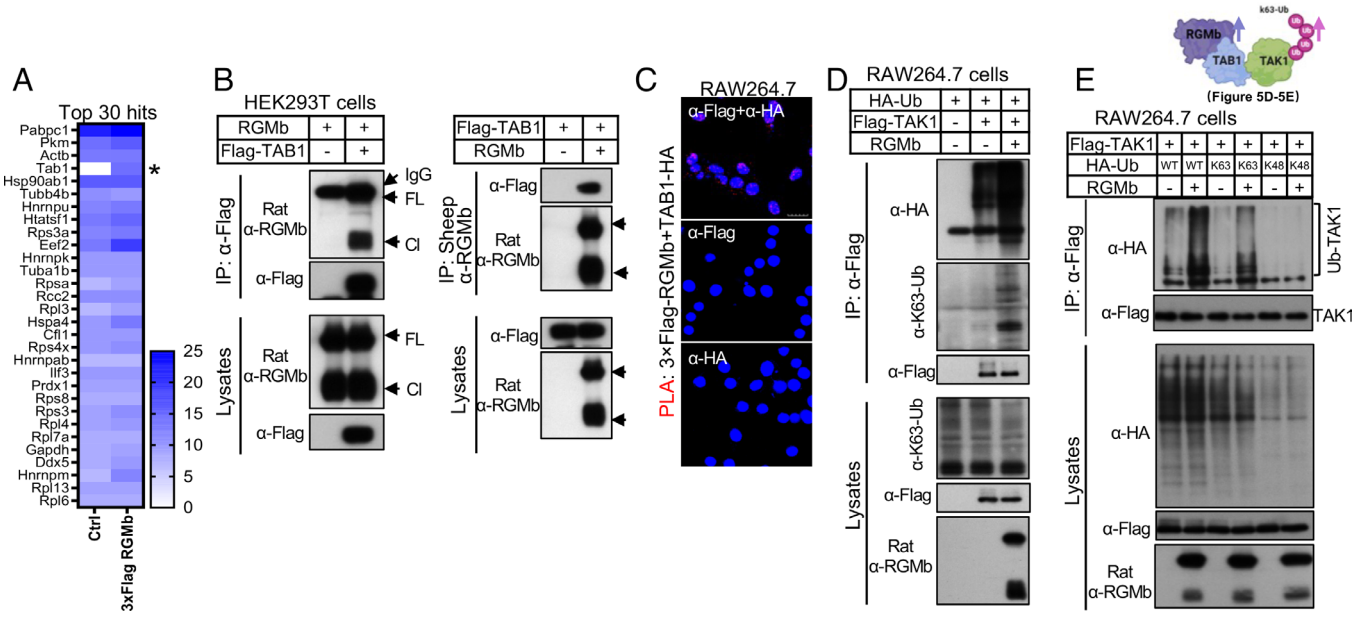

Fig. 5. RGMb directly interacted with TAB1 to promote TAK1 K63-linked polyubiquitination. (*A*) Heatmap showing the top 30 potential RGMb binding proteins in 3×Flag-RGMb RAW264.7 cells. (*B*) RGMb interacted with Flag-TAB1. HEK293T cells were transfected with RGMb plasmid in the absence or presence of Flag-TAB1 plasmid. Cell lysates were immunoprecipitated with anti-Flag antibody to capture TAB1 (*Left* panel). Reciprocal IP was performed (*Right* panel). Western blotting was performed on the whole lysates and precipitates as indicated. (*C*) Proximity ligation assay (PLA). RAW264.7 cells on coverslips were transfected with 3×Flag-RGMb and TAB1-HA plasmids. Cells were incubated with rabbit anti-HA antibody, mouse anti-Flag antibody, or both, followed by PLA staining. (*D*) RGMb promoted TAK1 polyubiquitination and K63-linked polyubiquitination in RAW264.7 macrophages. Cells were transfected with HA-Ub, in combination with control or Flag-TAK1 plasmids, and in the absence or presence of RGMb plasmids. Cell lysates were immunoprecipitated with anti-Flag antibody. (*E*) RGMb promoted the K63-linked but not K48-linked polyubiquitination of TAK1 in RAW264.7 macrophages. Cells were transfected with Flag-TAK1 and WT, K63 only, or K48 only HA-Ub plasmids in the absence or presence of RGMb plasmids. Cell lysates were immunoprecipitated with anti-Flag antibody.

inhibitor of apoptosis (XIAP) also contains a RING domain and displays an E3 ubiquitin ligase activity (44). Consistent with the previous findings (45, 46), TAB1 interacted with TRAF6 and XIAP (*SI Appendix*, Fig. S27 *B* and *C*). Unexpectedly, TAB1 did not interact with TRAF2 (*SI Appendix*, Fig. S27*A*). RGMb did not interact with TRAF2, TRAF6, or XIAP (*SI Appendix*, Fig. S27 *G–I*). Intriguingly, RGMb enhanced the interaction between TAB1 and TRAF6 as shown by IP and reciprocal IP (Fig. 6*A*) or PLA (Fig. 6*B*), whereas RGMb did not enhance the interaction between TAB1 and XIAP (*SI Appendix*, Fig. S27*D*). RGMb did not alter the interaction between TAK1 and TRAF6 (*SI Appendix*, Fig. S27*E*). TAK1 did not interact with XIAP regardless of the absence or presence of RGMb (*SI Appendix*, Fig. S27*F*).

To determine whether TRAF6 is responsible for the RGMb-induced TAK1 polyubiquitination, we used the TRAF6 inhibitor C25-140 that specifically targets TRAF6 E3 ligase activity (47). We found that RGMb-induced TAK1 polyubiquitination was abolished by C25-140 (Fig. 6*C*). Furthermore, basal and RGMb-stimulated TAK1 polyubiquitination was abolished when K158 of TAK1, a residue that can be polyubiquited by TRAF6 (41–43, 48) was mutated (TAK1 K158R) (Fig. 6*D*). To further confirm the role of the E3 ligase activity of TRAF6 in RGMb-induced TAK1 K63-linked polyubiquitination, we transfected RAW264.7 cells with plasmids for RING domain single point mutant (C70A-TRAF6), which inactivates the E3 ligase (49). We found that TRAF6 E3 ligase activity deficiency inhibited RGMb-induced TAK1 K63-linked polyubiquitination (Fig. 6*E*, compare lanes 4 and 2). These results suggest that RGMb promotes TRAF6-induced polyubiquitination of TAK1 at the Lys158 residue.

Given the role of RGMb in the K63-linked polyubiquitination of TAK1, we examined the effects of RGMb on TAK1 phosphorylation. Strikingly, RGMb overexpression highly increased the phosphorylation levels of TAK1 at Thr187 (Fig. 6*F*), while inhibition of RGMb decreased this phosphorylation (Fig. 6*G*) in RAW264.7 cells. TAK1 phosphorylation levels were much lower in Rgmb mKO than in control BMDMs (Fig. 6*H*). Importantly, the ratios of p-TAK1 and F4/80 double-positive macrophages to all F4/80 macrophages were reduced in the kidneys of Rgmb mKO mice compared to the kidneys of control mice after four low-dose Cisplatin treatments (Fig. 6*I*). Therefore, our results indicate that RGMb binds TAB1 and facilitates the interaction between TRAF6 and TAB1, thereby enhancing TAK1 polyubiquitination and phosphorylation.

TAK1 Promoted Macrophage Migration Both In Vitro and In Vivo. TAK1 has been found to promote migration of endothelial cells (50), neuronal cells (51), and ameloblastoma cells (24). However, the role of TAK1 in macrophage migration has not been studied. Since complete deletion of Tak1 in BMDMs results in spontaneous cell death (52), we used BMDMs from *Tak1*$^{flox/wt}$ mice to study the effects of TAK1 reduction. Infection of *Tak1*$^{flox/wt}$ BMDMs with Cre adenoviruses (Ad-Cre) reduced TAK1 expression by 40.3%, without induction of apoptosis (*SI Appendix*, Fig. S28 *A* and *B*). TAK1 reduction drastically decreased the migration of BMDM toward 10% FBS or CX3CL1 (Fig. 6*J* and *SI Appendix*, Fig. S28*C*). We also used (5Z)-7-oxozeanol (5Z7-OXO), a selective inhibitor of TAK1 (53), to inhibit TAK1 kinase activity. 5Z7-OXO treatment inhibited RAW264.7 migration (Fig. 6*K* and *SI Appendix*, Fig. S28*D*). Furthermore, TAK1 deficiency inhibited the invasion of BMDMs through Matrigel (Fig. 6*L* and *SI Appendix*, Fig. S29).

We labeled *Tak1*$^{flox/wt}$ BMDMs infected with Ad-GFP or Ad-Cre with PKH26 before the cells were injected into WT mice, followed by Cisplatin injection (*SI Appendix*, Fig. S30). Both flow cytometry and immunofluorescence indicated significantly decreased numbers of F4/80 and PKH26 double-positive cells in injured kidneys of mice that had received PKH26-labeled Tak1-deficient BMDMs compared to control BMDMs (Fig. 6*M* and *SI Appendix*, Fig. S30). Therefore, TAK1 increases macrophage migration and infiltration.

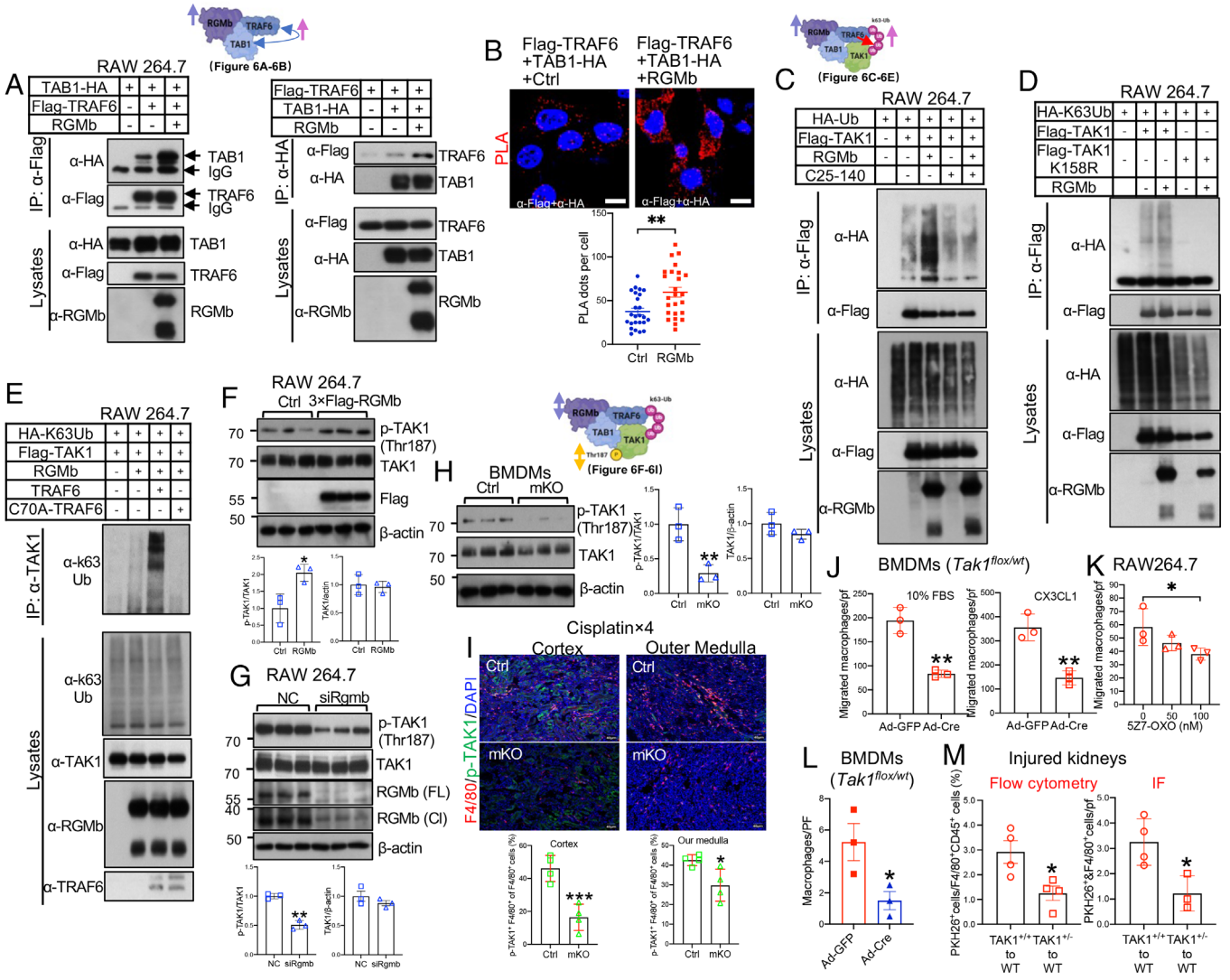

Fig. 6. RGMb enhanced the interaction between TRAF6 and TAB1 to promote TAK1 K63-linked polyubiquitination and phosphorylation and TAK1 deficiency inhibited macrophage infiltration. (*A*) RGMb facilitated the interaction between TRAF6 and TAB1. RAW264.7 macrophages were transfected with TAB1-HA, in combination with control or Flag-TRAF6, and in the absence or presence of RGMb. Cell lysates were immunoprecipitated with anti-Flag antibody (*Left* panels). In the reciprocal IP, RAW264.7 macrophages were transfected with Flag-TRAF6, in combination with control or TAB1-HA, and in the absence or presence of RGMb. (*B*) PLA for Flag-TRAF6 and TAB1-HA. RAW264.7 cells on coverslips were transfected with Flag-TRAF6 and TAB1-HA plasmids in the absence or presence of RGMb. PLA was performed (red, *Upper* panels). Red dots were counted in 25 cells per group (*Lower* panel). (*C*) Inhibition of TRAF6 activity abolished RGMb-induced TAK1 polyubiquitination. RAW264.7 cells were transfected with HA-Ub, in combination with control or Flag-TAK1, and in the absence or presence of RGMb. Cells were treated without or with the specific TRAF6 inhibitor C25-140 at 20 μM for 2 h. (*D*) RGMb promoted TAK1 K63-linked polyubiquitination on lysine residue 158 of TAK1. RAW264.7 cells were transfected with HA-K63Ub, in combination with control, Flag-TAK1, or Flag-TAK1 (K158R), and in the absence or presence of RGMb. (*E*) The E3 ligase-dead mutant C70A-TRAF6 inhibited RGMb-induced TAK1 K63-linked polyubiquitination. RAW264.7 cells were transfected with HA-K63Ub and Flag-TAK1 without or with WT-TRAF6 or C70A-TRAF6, and in the absence or presence of RGMb. (*F*) RGMb overexpression increased TAK1 phosphorylation. RAW264.7 macrophages were transfected with control or 3×Flag-RGMb plasmids. (*G*) Inhibition of RGMb expression decreased TAK1 phosphorylation. RAW264.7 macrophages were transfected with control (NC) or Rgmb siRNAs. (*H*) Deletion of Rgmb diminished TAK1 phosphorylation in BMDMs. Cell lysates from control and Rgmb mKO BMDMs were subjected to western blotting as indicated. (*I*) Decreased p-TAK1 and F4/80$^+$ double-positive cell numbers in the kidneys of Rgmb mKO mice after four low doses of Cisplatin. Frozen kidney sections were used for costaining for p-TAK1 (Thr187) (green) and F4/80 (red). n = 4 mice. (*J*) Tak1 deficiency reduced BMDM migration. BMDMs derived from *Tak1*$^{flox/wt}$ mice were infected with Ad-GFP or Ad-Cre before the cells were seeded on Transwell inserts (3 × 10^5 BMDMs/well). 10% FBS or CX3CL1 (100 ng/mL) was added into the lower chambers. 18 h later, migrated cells were counted. One well represents one animal. (*K*) Inhibition of TAK1 activity reduced RAW264.7 macrophage migration. Transwell migration assays were performed with RAW264.7 cells in the presence of increasing amounts of the specific TAK1 inhibitor 5Z7-OXO (0 to 100 nM) for 16 h. (*L*) Tak1 deficiency inhibited macrophage invasion. BMDMs (Tak1$^{flox/wt}$) were infected with Ad-GFP or Ad-Cre before they were seeded on Matrigel in a Transwell. CX3CL1 was added into the lower chamber. 24 h later, migrated BMDMs were counted. n = 3 mice. (*M*) Tak1 deficiency reduced the infiltration of BMDMs into injured kidneys. BMDMs derived from *Tak1*$^{flox/wt}$ mice were infected with Ad-GFP (Tak1$^{+/+}$) or Ad-Cre (Tak1$^{+/-}$) before they were labeled with PKH26 and injected through the tail vein into WT mice. Two days later, the mice were injected with Cisplatin. Labeled cells in the injured kidney were evaluated 3 d after Cisplatin injection by flow cytometry (*Left*) or immunofluorescence (*Right*). *P < 0.05; **P < 0.01; ***P < 0.001.

The TAK1/αTAT1 Cascade Mediated the Stimulatory Effects of RGMb on α-Tubulin Acetylation and Migration in Macrophages. α-tubulin acetylation is involved in microtubule stability and cell migration. αTAT1 is the enzyme that acetylates α-tubulin at Lys-40 (18, 21, 54). Recent studies have demonstrated that TAK1 phosphorylates αTAT1 at Ser237, which subsequently acetylates α-tubulin (26). We used a phospho-αTAT1 (Ser237) antibody, which was previously verified suitable for immunoprecipitation but not for western blotting (26), to perform immunoprecipitation on lysates from *Tak1*$^{flox/wt}$ BMDMs infected with Ad-GFP or Ad-Cre. We then immunoblotted immunoprecipitates with a pan-αTAT1 antibody. As expected,

αTAT1 phosphorylation levels were lower in Tak1 deficient BMDMs than in wild type BMDMs (Fig. 7*A* and *SI Appendix*, Fig. S31*A*). Acetylated (ac) tubulin levels were also decreased in Tak1 deficient BMDMs compared to wild type BMDMs (Fig. 7*B*). Inhibition of TAK1 by 5Z7-OXO reduced ac-tubulin levels in RAW264.7 cells (*SI Appendix*, Fig. S32*A*). These results confirm that the previously identified TAK1/αTAT1/α-tubulin cascade (26) exists in macrophages.

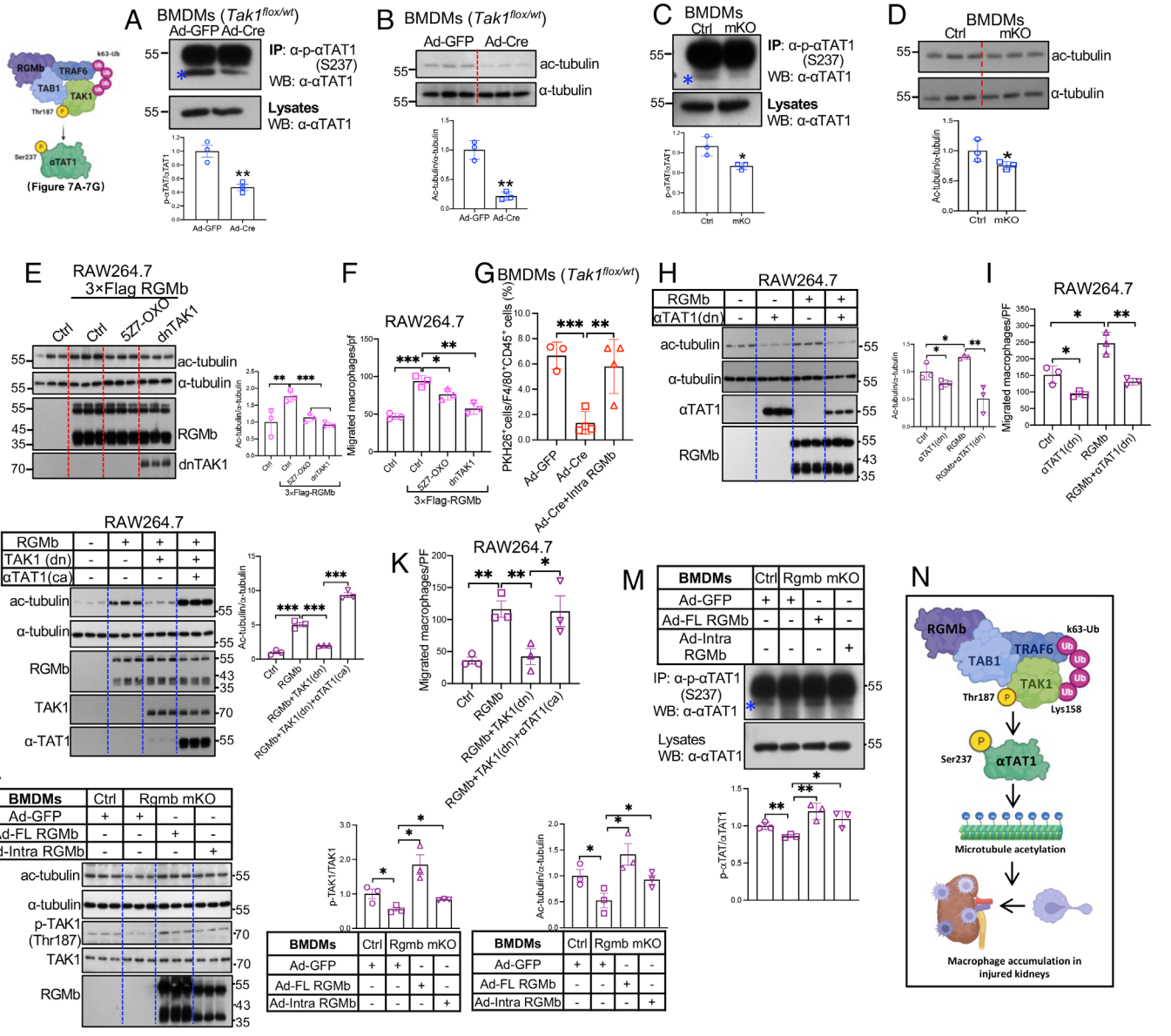

Fig. 7. TAK1 and αTAT1 mediated the effects of RGMb and TAK1 on α-tubulin acetylation and migration. (*A*) Tak1 deficiency decreased αTAT1 phosphorylation (S237) in BMDMs. BMDMs derived from *Tak1*$^{flox/wt}$ mice were infected with Ad-GFP or Ad-Cre before they were serum starved and then treated with CX3CL1 for 1 h. Cell lysates were immunoprecipitated with anti-p-αTAT1 antibody, and immunoblotted with anti-αTAT1 antibody. Only one of the three repeats is presented. Refer to *SI Appendix*, Fig. S31*A* for the three repeats. (*B*) Tak1 deficiency inhibited α-tubulin acetylation. BMDMs derived from *Tak1*$^{flox/wt}$ mice were infected with Ad-GFP or Ad-Cre before they were subjected to western blotting for α-tubulin acetylation at K40. (*C*) Ablation of Rgmb diminished αTAT1 phosphorylation (S237) in BMDMS. BMDMs derived from control and Rgmb mKO mice were serum starved and then treated with CX3CL1 for 1 h. Cell lysates were immunoprecipitated with anti-p-αTAT1 antibody. Only one of the three repeats is presented. Refer to *SI Appendix*, Fig. S31*B* for the three repeats. (*D*) Ablation of Rgmb inhibited α-tubulin acetylation in BMDMs. BMDMs derived from control and Rgmb mKO mice were serum starved. (*E* and *F*) Induction of α-tubulin acetylation and migration by RGMb were blocked by inhibition of TAK1. RAW264.7 macrophages were transfected with control or 3×Flag-RGMb plasmids in the absence or presence of dnTAK1. Cells then were treated with vehicle (DMSO) or 5Z7-OXO (100 nM) for 16 h (*E*). Cells were also subjected to Transwell migration for 16 h (*F*). n = 3 wells. (*G*) Decreased infiltration of BMDMs into injured kidneys by Tak1 deficiency was rescued by forced expression of Intra RGMb. BMDMs derived from *Tak1*$^{flox/wt}$ were infected with Ad-GFP, Ad-Cre, or Ad-Cre plus Ad-Intra RGMb before they were labeled with PKH26 and injected through the tail vein into WT mice. Two days later, the mice were injected with Cisplatin. Labeled cells in the injured kidney were evaluated 3 d after Cisplatin injection by flow cytometry. n = 3 to 4 mice. (*H* and *I*) RGMb-induced α-tubulin acetylation and migration were abolished by αTAT1 inhibition. RAW264.7 macrophages were transfected with control or RGMb plasmids in the absence or presence of αTAT1(dn) (*H*). Cells were also subjected to Transwell migration for 16 h (*I*). (*J* and *K*) Induction of α-tubulin acetylation and migration by RGMb was dependent on TAK1 and αTAT1. RAW264.7 macrophages were transfected with control or RGMb plasmids, in the absence or presence of TAK1(dn), and in combination without or with αTAT1 (ca) (*J*). Cells were also subjected to Transwell migration for 16 h (*K*). (*L*) Decreased TAK1 phosphorylation and α-tubulin acetylation induced by Rgmb deletion in BMDMs was rescued by reintroduction of FL RGMb or Intra RGMb. Control BMDMs were infected with Ad-GFP. Rgmb mKO BMDMs were infected with Ad-GFP, Ad-FL RGMb, or Ad-Intra RGMb before the cells were harvested for western blotting as indicated. n = 3 mice. (*M*) Decreased p-αTAT1(S237) levels in Rgmb mKO BMDMs were rescued by reintroduction of FL RGMb or Intra RGMb. Control BMDMs were infected with Ad-GFP. Rgmb mKO BMDMs were infected with Ad-GFP, Ad-FL RGMb, or Ad-Intra RGMb and treated with CX3CL1 at 100 ng/mL for 1 h before the cells were harvested. Cell lysates were immunoprecipitated with anti-p-αTAT1(S237) antibody, and immunoblotted with anti-αTAT1 antibody. n = 3 mice. (*N*) Schematic diagram summarizing the mechanisms of action of RGMb in regulating macrophage migration. *P < 0.05; **P < 0.01; ***P < 0.001.

Strikingly, phospho-αTAT1 levels were lower in Rgmb mKO BMDMs than in control BMDMs (Fig. 7*C* and *SI Appendix*, Fig. S31*B*). Ac-tubulin levels were also lowered in Rgmb mKO compared to control BMDMs no matter whether the cells are serum starved (Fig. 7*D*) or exposed to 10% FBS or CX3CL1 (*SI Appendix*, Fig. S32*B*). RGMb, Intra RGMb (*SI Appendix*, Fig. S32*C*), or cotransfection of the N- and C-terminuses of RGMb (*SI Appendix*, Fig. S32*D*) increased phospho-TAK1 and ac-tubulin levels while the N-terminus had no effects (*SI Appendix*, Fig. S32*E*) in RAW264.7 cells. Conversely, inhibition of RGMb lowered both TAK1 phosphorylation and α-tubulin acetylation levels in RAW264.7 cells (*SI Appendix*, Fig. S32*F*). These results suggest that RGMb activates the TAK1/αTAT1/α-tubulin cascade.

To determine the role of TAK1 in RGMb's actions on α-tubulin acetylation and macrophage migration, we transfected RAW264.7 cells with RGMb plasmids in the absence or presence of 5Z7-OXO or dnTAK1 (TAK1 K63W). RGMb-induced α-tubulin acetylation and migration both were attenuated by either 5Z7-OXO treatment or dnTAK1 expression (Fig. 7 *E* and *F* and *SI Appendix*, Fig. S33*A*). siRNA-mediated inhibition of RGMb decreased α-tubulin acetylation and migration in RAW264.7 macrophages, which were rescued by cotransfection with TAK1 and TAB1 (*SI Appendix*, Fig. S33 *B* and *C*). Importantly, the decreased infiltration of Tak1$^{+/-}$ BMDMs into injured kidneys was restored to control levels by overexpression of Intra RGMb in the cells (Fig. 7*G* and *SI Appendix*, Fig. S34). Therefore, TAK1 indeed mediates RGMb's regulation on α-tubulin acetylation and migration in macrophages.

TAK1 phosphorylates αTAT1 at Ser237, which acetylates α-tubulin (26). Interestingly, both basal and RGMb-induced α-tubulin acetylation (Fig. 7*H*) and migration (Fig. 7*I* and *SI Appendix*, Fig. S35*A*) in RAW264.7 cells were reduced by non-phosphorylatable or dominant-negative (dn) αTAT1 (S237A). Conversely, the decreased α-tubulin acetylation (*SI Appendix*, Fig. S35*B*) and migration (*SI Appendix*, Fig. S35*C*) induced by RGMb knockdown in RAW264.7 cells were restored by constitutively active (ca) phosphomimetic αTAT1 mutant (S237E). Furthermore, RGMb-induced α-tubulin acetylation (Fig. 7*J*) and migration (Fig. 7*K* and *SI Appendix*, Fig. S35*D*) in RAW264.7 cells were inhibited by dnTAK1, and this inhibition was abolished by cotransfection with ca-αTAT1. Importantly, reconstitution of either FL or Intra RGMb in Rgmb mKO BMDMs restored the TAK1 phosphorylation (Fig. 7*L*), αTAT1 phosphorylation (Fig. 7*M*), α-tubulin acetylation (Fig. 7*L*), and migration (Fig. 3*B*) in vitro and infiltration into injured kidneys (Fig. 2*F*). Therefore, αTAT1 mediates the α-tubulin acetylation and macrophage migration induced by RGMb/TAK1 (Fig. 7*N*).

Discussion

In the present study, we demonstrated that RGMb plays a critical role in macrophage migration. RGMb-mediated macrophage infiltration contributes to kidney inflammation and subsequent tubular injury and renal fibrosis in a variety of mouse kidney injury models (Fig. 7*N*). Although RGMb is a GPI-anchored membrane protein, more RGMb protein is found inside cells than on plasma membrane (7–9, 55). We found that the activity of RGMb on macrophage migration can be mediated by intracellular RGMb. RGMb directly interacted with TAB1 to promote macrophage migration by activating the TRAF6/TAB1 (TAK1)/α-TAT1/α tubulin cascade, thereby regulating cell shape and migration.

It has been demonstrated that blockade of RGMb by anti-RGMb mAb alleviated airway inflammation (8), and mitigated graft-versus-host disease and DSS-induced inflammatory bowel disease (16). Therefore, the extracellular RGMb forms, i.e., soluble and/or cell surface RGMb, appeared to enhance inflammatory responses. In the present study, we showed that intracellular RGMb in macrophages is also proinflammatory. However, our previous studies indicated an anti-inflammatory role for RGMb since global deletion of Rgmb led to spontaneous lung inflammation (12), and inducible global deletion of Rgmb in adult mice heightened DSS-induced intestinal inflammation (17). These seemingly contradictory observations highlight the complexity of the biological functions of RGMb and the necessity of dissecting the roles of RGMb in different cell types especially in various immune cells and in cell–cell communications.

We used LysM-Cre to generate myeloid-specific Rgmb knockout (mKO) mice. Rgmb mKO mice were grossly normal and survived to adulthood. Of note, deletion of Rgmb in CD4$^+$ T cells did not result in lethality either (15). These results suggest that the postnatal lethality induced by global Rgmb deletion involves aberrant functions of multiple cell types. The mechanisms underlying the postnatal death in global Rgmb KO mice are under active investigation.

RGMb expression in IMs was decreased, and the number of IMs was also reduced in the kidneys of Rgmb mKO mice compared to the kidneys of WT mice. Consistent with the targeting specificity of LysM-Cre (56, 57), RGMb expression in KRMs was not altered by LysM-Cre. The number of KRMs tended to be decreased in Rgmb mKO kidneys. We suspect that this decrease may not be a direct effect of KRM RGMb, but most likely is a result of the altered inflammatory microenvironment induced by decreased IM numbers.

We provided evidence that intracellular RGMb promoted macrophage migration and infiltration and mediated kidney injury. We found that overexpression of an intracellular form of RGMb was sufficient to promote the migration of RAW264.7 macrophages, and reconstitution of Rgmb mKO BMDMs with intracellular RGMb brought the defective migration of Rgmb mKO BMDMs to control levels both in vitro and in vivo. Furthermore, we were able to show that depletion of macrophages prevented Cisplatin-induced kidney injury, and transfer of Rgmb mKO BMDMs into macrophage-depleted mice failed to restore Cisplatin-induced kidney injury while transfer of WT BMDMs did. Consistent with a role for RGMb in macrophage migration, reconstitution of Rgmb mKO BMDMs with intracellular RGMb restored Cisplatin-induced kidney injury to WT levels.

Another important finding of the present study is that RGMb directly interacted with TAB1. RGMb promoted the interaction between TRAF6 and TAB1, thus enhancing TRAF6-mediated TAK1 K63-linked polyubiquitination and TAK1 phosphorylation at Thr187. As a member of the MAP3K family, TAK1 together with TAB1 is critically involved in activation of multiple innate and adaptive immune signaling cascades including the NFκB and MAPK pathways (39). However, whether TAK1 plays a role in macrophage migration was unknown. In the present study, we revealed that TAK1 promoted macrophage migration in vitro and facilitated the infiltration of macrophages into injured kidneys in vivo. Furthermore, TAK1 mediated RGMb-induced macrophage migration and infiltration. Therefore, our results suggest that RGMb promotes macrophage migration by activating TAK1.

It has been well established that α-tubulin acetylation plays a critical role in cell cytoskeleton remodeling, intracellular transport, and cell migration (19), A previous study demonstrated that TAK1 phosphorylated α-TAT1, which in turn promoted α-tubulin acetylation (26). We now have extended this pathway by adding RGMb upstream of TAK1. Furthermore, we found that phospho-α-TAT1

mediated the α-tubulin acetylation and migration induced by RGMb in macrophages.

As an adhesion structure at the cell–matrix interface, podosomes are vital for macrophages to perform matrix degradation and migration through tissue compartments. In the present study, we used a STED superresolution microscope to capture 3D structures of podosomes in control and Rgmb mKO BMDMs. The structure of podosomes was found to be defective in Rgmb mKO BMDMs. The podosome numbers were diminished by Rgmb deletion. A previous study showed that the release of the guanine nucleotide exchange factor GEF-H1 from microtubules, a process that was controlled by α-tubulin K40 acetylation, was crucial in podosome turnover and cell migration (25). In the present study, we showed RGMb promoted α-tubulin K40 acetylation. Whether the defects in the podosomes of Rgmb mKO BMDMs resulted from the decreased microtubule acetylation is an open question to be addressed.

In our LPS-induced sepsis model, macrophage infiltration was found to be decreased not only in the kidneys and but also in the livers of Rgmb KO mice when compared to control mice. Therefore, RGMb-mediated macrophage infiltration may be generalizable to other organs.

Taken together, we found that RGMb is an important intrinsic factor that drives macrophage infiltration into injured kidneys. RGMb promotes macrophage migration by activating the TRAF6/TAB1 (TAK1)/α-TAT1/α-tubulin cascade (Fig. 7*N*). These findings suggest that targeting RGMb may be an effective therapy for the treatment of kidney inflammation and fibrosis.

Materials and Methods

Mice. Myeloid cell–specific Rgmb knockout (Rgmb mKO) mice were generated by breeding *RGMb*$^{flox/flox}$ mice with *LysM-Cre* knockin mice on C57BL/6 background. All animal studies were approved by the Animal Experimentation Ethics Committee (AEEC) of The Chinese University of Hong Kong (Ref. No. 21-317-GRF). Animals were housed in the Laboratory Animal Services Centre (LASEC) at The Chinese University of Hong Kong.

scRNA-Seq Analysis of Whole Kidneys. Single cells were loaded onto 10X Chromium System (10X Genomics) by the Single Cell Omics Core in School of Biomedical Science, The Chinese University of Hong Kong. Detailed materials and methods can be found in *SI Appendix*.

Data, Materials, and Software Availability. scRNA-seq data have been deposited in Gene Expression Omnibus (GSE268818) (58).

ACKNOWLEDGMENTS. pCMV-Flag-TAB1 plasmid was provided by Dr. Jun Ninomiya-Tsuji (North Carolina State University). Flag-TAK1 plasmid was provided by Dr. Yujie Deng and Dr. Kingston Mak (Guangzhou Laboratory). We thank Dr. Binbin Chen and Dr. Wenjing Liu for generating the 2×Flag-mRGMb C-terminus and RGMb DP/AA plasmids respectively. We thank Dr. Joaquim Vong for help with the single-cell RNA sequencing assay, and Dr. Jacque Ip for help with the stimulated emission depletion microscopy. This work was supported by General Research Funds 14102620, 14112121, 14108922, and 14111523, Hong Kong Research Grants Council (to Y.X.); Health and Medical Research Funds 05161376, 07180636, and 08190376, Hong Kong Health Bureau (to Y.X.); The Strategic Seed Funding for Collaborative Research Scheme NL/SSFCRS2022/0674/22en, The Chinese University of Hong Kong (to Y.X.); NIH Grants P50CA101942 and AI056299 (to G.J.F.); Shenzhen Longgang District Science and Technology Innovation Special Fund (LGKCYLWS2024-5) (to C.X.); and National Natural Science Foundation of China-Young Scientist Fund 82400818 (to Y.K.). Y.K. was supported in part by the Faculty Postdoctoral Fellowship (FPFS/20-21/30 and FPFS/21-22/R/11) and the Postdoctoral Fellowship Scheme (WW/PDFS2023/0661/23en), The Chinese University of Hong Kong.

Author affiliations: [a]School of Biomedical Sciences, Faculty of Medicine, The Chinese University of Hong Kong, Hong Kong, China; [b]Shenzhen Research Institute, The Chinese University of Hong Kong, Shenzhen 518057, China; [c]AIDS Institute and Department of Microbiology, School of Clinical Medicine, Li Ka Shing Faculty of Medicine, The University of Hong Kong, Hong Kong, China; [d]Department of Nephrology, Longgang Central Hospital of Shenzhen, Shenzhen 518116, China; [e]School of Optometry, The Hong Kong Polytechnic University, Hung Hom, Kowloon, Hong Kong, China; [f]Guangdong Provincial Key Laboratory of Autophagy and Major Chronic Non-Communicable Diseases, Affiliated Hospital, Guangdong Medical University, Zhanjiang 524023, China; [g]The Key Laboratory of Model Animal for Disease Study of Ministry of Education, Model Animal Research Center, Nanjing University, Nanjing 210061, China; [h]Department of Pharmacology, College of Medicine, University of Arizona, Tucson, AZ 85724; [i]Department of Medical Oncology, Dana-Farber Cancer Institute, Harvard Medical School, Boston, MA 02215; and [j]Key Laboratory for Regenerative Medicine, Ministry of Education, School of Biomedical Sciences, Faculty of Medicine, The Chinese University of Hong Kong, Hong Kong, China

1. K. J. Foreman *et al.*, Forecasting life expectancy, years of life lost, and all-cause and cause-specific mortality for 250 causes of death: Reference and alternative scenarios for 2016–40 for 195 countries and territories. *Lancet* **392**, 2052–2090 (2018).
2. B. D. Humphreys, Mechanisms of renal fibrosis. *Annu. Rev. Physiol.* **80**, 309–326 (2018).
3. S. M. Yu, J. V. Bonventre, Acute kidney injury and maladaptive tubular repair leading to renal fibrosis. *Curr. Opin. Nephrol. Hypertens.* **29**, 310–318 (2020).
4. X. M. Meng, D. J. Nikolic-Paterson, H. Y. Lan, Inflammatory processes in renal fibrosis. *Nat. Rev. Nephrol.* **10**, 493–503 (2014).
5. P. M. Tang, D. J. Nikolic-Paterson, H. Y. Lan, Macrophages: Versatile players in renal inflammation and fibrosis. *Nat. Rev. Nephrol.* **15**, 144–158 (2019).
6. C. Siebold, T. Yamashita, P. P. Monnier, B. K. Mueller, R. J. Pasterkamp, RGMs: Structural insights, molecular regulation, and downstream signaling. *Trends Cell Biol.* **27**, 365–378 (2017).
7. Y. Xiao *et al.*, RGMb is a novel binding partner for PD-L2 and its engagement with PD-L2 promotes respiratory tolerance. *J. Exp. Med.* **211**, 943–959 (2014).
8. S. Yu *et al.*, Blockade of RGMb inhibits allergen-induced airways disease. *J. Allergy Clin. Immunol.* **144**, 94–108.e111 (2019).
9. H. Harada *et al.*, Extracellular phosphorylation drives the formation of neuronal circuitry. *Nat. Chem. Biol.* **15**, 1035–1042 (2019).
10. M. S. Kim *et al.*, A draft map of the human proteome. *Nature* **509**, 575–581 (2014).
11. P. Rotwein, Variation in the repulsive guidance molecule family in human populations. *Physiol. Rep.* **7**, e13959 (2019).
12. Y. Xia *et al.*, Dragon (repulsive guidance molecule b) inhibits IL-6 expression in macrophages. *J. Immunol.* **186**, 1369–1376 (2011).
13. W. Liu *et al.*, Dragon (repulsive guidance molecule RGMb) inhibits E-cadherin expression and induces apoptosis in renal tubular epithelial cells. *J. Biol. Chem.* **288**, 31528–31539 (2013).
14. W. Liu *et al.*, RGMb protects against acute kidney injury by inhibiting tubular cell necroptosis via an MLKL-dependent mechanism. *Proc. Natl. Acad. Sci. U.S.A.* **115**, E1475–E1484 (2018).
15. J. S. Park *et al.*, Targeting PD-L2-RGMb overcomes microbiome-related immunotherapy resistance. *Nature* **617**, 377–385 (2023).
16. M. Perez-Cruz *et al.*, Immunoregulatory effects of RGMb in gut inflammation. *Front. Immunol.* **13**, 960329 (2022).
17. Y. Shi *et al.*, Repulsive guidance molecule b deficiency induces gut microbiota dysbiosis and increases the susceptibility to intestinal inflammation in mice. *Front. Microbiol.* **12**, 648915 (2021).
18. G. G. Gundersen, J. C. Bulinski, Selective stabilization of microtubules oriented toward the direction of cell migration. *Proc. Natl. Acad. Sci. U.S.A.* **85**, 5946–5950 (1988).
19. C. Janke, J. C. Bulinski, Post-translational regulation of the microtubule cytoskeleton: Mechanisms and functions. *Nat. Rev. Mol. Cell Biol.* **12**, 773–786 (2011).
20. B. P. Bouchet, A. Akhmanova, Microtubules in 3D cell motility. *J. Cell Sci.* **130**, 39–50 (2017).
21. B. Bance, S. Seetharaman, C. Leduc, B. Boeda, S. Etienne-Manneville, Microtubule acetylation but not detyrosination promotes focal adhesion dynamics and astrocyte migration. *J. Cell Sci.* **132**, jcs225805 (2019).
22. N. Kalebic *et al.*, alphaTAT1 is the major alpha-tubulin acetyltransferase in mice. *Nat. Commun.* **4**, 1962 (2013).
23. A. E. Boggs *et al.*, alpha-Tubulin acetylation elevated in metastatic and basal-like breast cancer cells promotes microtentacle formation, adhesion, and invasive migration. *Cancer Res.* **75**, 203–215 (2015).
24. S. Yoshimoto, H. Morita, K. Okamura, A. Hiraki, S. Hashimoto, alphaTAT1-induced tubulin acetylation promotes ameloblastoma migration and invasion. *Lab Invest.* **102**, 80–89 (2022).
25. S. Seetharaman *et al.*, Microtubules tune mechanosensitive cell responses. *Nat. Mater.* **21**, 366–377 (2022).
26. N. Shah *et al.*, TAK1 activation of alpha-TAT1 and microtubule hyperacetylation control AKT signaling and cell growth. *Nat. Commun.* **9**, 1696 (2018).
27. A. F. Malone *et al.*, Harnessing expressed single nucleotide variation and single cell RNA sequencing to define immune cell chimerism in the rejecting kidney transplant. *J. Am. Soc. Nephrol.* **31**, 1977–1986 (2020).
28. Y. Kirita, H. Wu, K. Uchimura, P. C. Wilson, B. D. Humphreys, Cell profiling of mouse acute kidney injury reveals conserved cellular responses to injury. *Proc. Natl. Acad. Sci. U.S.A.* **117**, 15874–15883 (2020).
29. J. Fu *et al.*, The single-cell landscape of kidney immune cells reveals transcriptional heterogeneity in early diabetic kidney disease. *Kidney Int.* **102**, 1291–1304 (2022).
30. C. Schulz *et al.*, A lineage of myeloid cells independent of Myb and hematopoietic stem cells. *Science* **336**, 86–90 (2012).
31. N. S. Shin *et al.*, Arginase-1 is required for macrophage-mediated renal tubule regeneration. *J. Am. Soc. Nephrol.* **33**, 1077–1086 (2022).
32. K. A. Zimmerman *et al.*, Single-cell RNA sequencing identifies candidate renal resident macrophage gene expression signatures across species. *J. Am. Soc. Nephrol.* **30**, 767–781 (2019).

33. W. Yao *et al.*, Single cell RNA sequencing identifies a unique inflammatory macrophage subset as a druggable target for alleviating acute kidney injury. *Adv. Sci. (Weinh.)* **9**, e2103675 (2022).
34. C. Auffray *et al.*, Monitoring of blood vessels and tissues by a population of monocytes with patrolling behavior. *Science* **317**, 666–670 (2007).
35. M. Trizzino *et al.*, EGR1 is a gatekeeper of inflammatory enhancers in human macrophages. *Sci. Adv.* **7**, eaaz8836 (2021).
36. E. Kowenz-Leutz, P. Herr, K. Niss, A. Leutz, The homeobox gene GBX2, a target of the myb oncogene, mediates autocrine growth and monocyte differentiation. *Cell* **91**, 185–195 (1997).
37. S. Linder, M. Aepfelbacher, Podosomes: Adhesion hot-spots of invasive cells. *Trends Cell Biol.* **13**, 376–385 (2003).
38. D. A. Murphy, S. A. Courtneidge, The "ins" and "outs" of podosomes and invadopodia: Characteristics, formation and function. *Nat. Rev. Mol. Cell Biol.* **12**, 413–426 (2011).
39. H. Mukhopadhyay, N. Y. Lee, Multifaceted roles of TAK1 signaling in cancer. *Oncogene* **39**, 1402–1413 (2020).
40. H. Shibuya *et al.*, TAB1: An activator of the TAK1 MAPKKK in TGF-beta signal transduction. *Science* **272**, 1179–1182 (1996).
41. Y. Fan *et al.*, Lysine 63-linked polyubiquitination of TAK1 at lysine 158 is required for tumor necrosis factor alpha- and interleukin-1beta-induced IKK/NF-kappaB and JNK/AP-1 activation. *J. Biol. Chem.* **285**, 5347–5360 (2010).
42. A. Sorrentino *et al.*, The type I TGF-beta receptor engages TRAF6 to activate TAK1 in a receptor kinase-independent manner. *Nat. Cell Biol.* **10**, 1199–1207 (2008).
43. N. Ahmed *et al.*, The E3 ligase Itch and deubiquitinase Cyld act together to regulate Tak1 and inflammation. *Nat. Immunol.* **12**, 1176–1183 (2011).
44. S. Kaur, F. Wang, M. Venkatraman, M. Arsura, X-linked inhibitor of apoptosis (XIAP) inhibits c-Jun N-terminal kinase 1 (JNK1) activation by transforming growth factor beta1 (TGF-beta1) through ubiquitin-mediated proteosomal degradation of the TGF-beta1-activated kinase 1 (TAK1). *J. Biol. Chem.* **280**, 38599–38608 (2005).
45. K. Yamaguchi *et al.*, XIAP, a cellular member of the inhibitor of apoptosis protein family, links the receptors to TAB1-TAK1 in the BMP signaling pathway. *EMBO J.* **18**, 179–187 (1999).
46. M. C. Walsh, G. K. Kim, P. L. Maurizio, E. E. Molnar, Y. Choi, TRAF6 autoubiquitination-independent activation of the NFkappaB and MAPK pathways in response to IL-1 and RANKL. *PLoS ONE* **3**, e4064 (2008).
47. J. K. Brenke *et al.*, Targeting TRAF6 E3 ligase activity with a small-molecule inhibitor combats autoimmunity. *J. Biol. Chem.* **293**, 13191–13203 (2018).
48. A. Lamb *et al.*, Helicobacter pylori CagA activates NF-kappaB by targeting TAK1 for TRAF6-mediated Lys 63 ubiquitination. *EMBO Rep.* **10**, 1242–1249 (2009).
49. B. Lamothe *et al.*, Site-specific Lys-63-linked tumor necrosis factor receptor-associated factor 6 auto-ubiquitination is a critical determinant of I kappa B kinase activation. *J. Biol. Chem.* **282**, 4102–4112 (2007).
50. S. Morioka *et al.*, TAK1 kinase signaling regulates embryonic angiogenesis by modulating endothelial cell survival and migration. *Blood* **120**, 3846–3857 (2012).
51. F. Zhang *et al.*, A novel c-Jun N-terminal kinase (JNK) signaling complex involved in neuronal migration during brain development. *J. Biol. Chem.* **291**, 11466–11475 (2016).
52. A. A. Ajibade *et al.*, TAK1 negatively regulates NF-kappaB and p38 MAP kinase activation in Gr-1+CD11b+ neutrophils. *Immunity* **36**, 43–54 (2012).
53. J. Ninomiya-Tsuji *et al.*, A resorcylic acid lactone, 5Z-7-oxozeaenol, prevents inflammation by inhibiting the catalytic activity of TAK1 MAPK kinase kinase. *J. Biol. Chem.* **278**, 18485–18490 (2003).
54. T. Aoki *et al.*, Intraflagellar transport 20 promotes collective cancer cell invasion by regulating polarized organization of Golgi-associated microtubules. *Cancer Sci.* **110**, 1306–1316 (2019).
55. J. Li, L. Ye, H. G. Kynaston, W. G. Jiang, Repulsive guidance molecules, novel bone morphogenetic protein co-receptors, are key regulators of the growth and aggressiveness of prostate cancer cells. *Int. J. Oncol.* **40**, 544–550 (2012).
56. B. E. Clausen, C. Burkhardt, W. Reith, R. Renkawitz, I. Forster, Conditional gene targeting in macrophages and granulocytes using LysMcre mice. *Transgenic Res.* **8**, 265–277 (1999).
57. T. Lei *et al.*, Defining newly formed and tissue-resident bone marrow-derived macrophages in adult mice based on lysozyme expression. *Cell Mol. Immunol.* **19**, 1333–1346 (2022).
58. Y. Xia, Y. Kong, M. Yue, Gene expression profile at single cell level of kidneys from RGMb flox/flox Lyz2 cre (RGMb mKO) & Lyz2 cre (Ctrl) mice with or with cisplatin (20 mg/KG body weight for 72 h). Gene Expression Omnibus. https://www.ncbi.nlm.nih.gov/geo/query/acc.cgi?acc=GSE268818. Deposited 31 May 2024.